

2012-5-25

Modifying the Electronic Properties of Single-Walled Carbon Nanotubes using Designed Surfactant Peptides

Dinushi R. Samarajewa, *et al.*

© 2012 The Royal Society of Chemistry

Cite this: *Nanoscale*, 2012, **4**, 4544

www.rsc.org/nanoscale

PAPER

Modifying the electronic properties of single-walled carbon nanotubes using designed surfactant peptides†

Dinushi R. Samarajewa, Gregg R. Dieckmann, Steven O. Nielsen and Inga H. Musselman*

Received 22nd February 2012, Accepted 25th May 2012

DOI: 10.1039/c2nr30423f

The electronic properties of carbon nanotubes can be altered significantly by modifying the nanotube surface. In this study, single-walled carbon nanotubes (SWCNTs) were functionalized noncovalently using designed surfactant peptides, and the resultant SWCNT electronic properties were investigated. These peptides have a common amino acid sequence of X(Valine)₅(Lysine)₂, where X indicates an aromatic amino acid containing either an electron-donating or electron-withdrawing functional group (*i.e.* *p*-amino-phenylalanine or *p*-cyano-phenylalanine). Circular dichroism spectra showed that the surfactant peptides primarily have random coil structures in an aqueous medium, both alone and in the presence of SWCNTs, simplifying analysis of the peptide/SWCNT interaction. The ability of the surfactant peptides to disperse individual SWCNTs in solution was verified using atomic force microscopy and ultraviolet-visible-near-infrared spectroscopy. The electronic properties of the surfactant peptide/SWCNT composites were examined using the observed nanotube Raman tangential band shifts and the observed additional features near the Fermi level in the scanning tunneling spectroscopy dI/dV spectra. The results revealed that SWCNTs functionalized with surfactant peptides containing electron-donor or electron-acceptor functional groups showed n-doped or p-doped altered electronic properties, respectively. This work unveils a facile and versatile approach to modify the intrinsic electronic properties of SWCNTs using a simple peptide structure, which is easily adaptable to obtain peptide/SWCNT composites for the design of tunable nanoscale electronic devices.

1. Introduction

SWCNTs, which are comprised of a single cylindrical layer of sp^2 -hybridized carbon atoms, show unique electronic, thermal, and mechanical properties.¹ These properties imbue SWCNTs with their potential use as field-effect transistors, (bio)sensors, nanowires, mechanical fibers, energy storage devices, probe tips, and viable drug delivery vehicles.^{2–4} SWCNTs are identified as strong candidates for nanodevice applications due to the presence of both metallic and semiconducting tube types and their

nanometer dimensions. Furthermore, covalent and noncovalent modifications of carbon nanotubes have increased their applicability in carbon-based nanoelectronics.^{5,6} Particularly, altering SWCNT electronic properties *via* doping with electron-donors or electron-acceptors is intriguing, because it not only enhances the electrical and thermal conductivity of SWCNTs, but also provides control over their intrinsic electronic properties.^{7–19} Towards this end, various routes have been examined in order to alter the electronic structure of carbon nanotubes. For example, several well-known methods for doping carbon nanotubes include adsorption of electron donor–acceptor molecules onto nanotube surfaces,^{8–11} intercalation of donor–acceptor atoms in the interstitial spaces of nanotube bundles,¹² encapsulation of donor–acceptor molecules inside nanotube hollow cores,¹³ and substitution of the carbon atoms in the lattice with heteroatoms.^{14,15} Among these methods, substitutional doping requires the removal of carbon atoms from the inherent sp^2 network resulting in defective nanotube surfaces.¹⁵ Conversely, the other routes maintain the sp^2 -hybridized structure owing to the noncovalent nature of the interaction between the dopants and the carbon nanotubes and hence are preferred for many applications.

The current study examines the noncovalent functionalization of SWCNTs by short designed amphiphilic peptides, known as

Department of Chemistry, The University of Texas at Dallas, 800 West Campbell Road, Richardson, Texas 75080, USA. E-mail: imusselm@utdallas.edu; Fax: +1 972 883 2925; Tel: +1 972 883 2706

† Electronic supplementary information (ESI) available: Characteristics of the surfactant peptides; molecular weights and retention times; determination of molar extinction coefficients of aromatic test amino acids; determination of optimum surfactant peptide concentration and centrifugation speed for the preparation of SWCNT dispersions; absorption spectra of surfactant peptide/SWCNT dispersions as a function of centrifugation speed; chirality assignments of surfactant peptide/SWCNT composites and corresponding absorption peak shifts; reproducibility of Raman G-band peak positions of surfactant peptide/SWCNT composites; STM/STS data acquisition from standard substrates and surfactant peptide controls; preparation of 1,2-dichloroethane/SWCNT dispersions; peak positions of additional features near the Fermi level observed in STS dI/dV spectra of SWCNTs. See DOI: 10.1039/c2nr30423f

surfactant peptides, bearing electron-donating or electron-withdrawing groups. In this paper, we will show that SWCNTs coated with these peptides have altered electronic properties, wherein the SWCNTs are n-doped or p-doped depending on the aromatic group in the adsorbed peptide. Previous reports provide evidence for alterations of SWCNT electronic properties by the adsorption of small organic molecules with electron-donating or electron-withdrawing functionalities, such as aniline, nitro-benzene, tetracyanoquinodimethane, and tetrathiafulvalene.^{8–10} The noncovalent functionalization of SWCNTs with polymers, such as polyimides containing nitrile functionalized aromatic rings,¹⁶ polyethylenimine,¹⁷ and poly(3-hexyl-thiophene),¹⁸ also revealed the ability of adsorbed polymers to dope carbon nanotubes. Recently, Poenitzsch *et al.* examined another route to dope SWCNTs using designed α -helical peptides.¹⁹ Here, SWCNTs were noncovalently functionalized with amphiphilic α -helical peptides containing either an electron-donating (hydroxyl) or an electron-withdrawing (nitro) group in the aromatic side chain. Additional peaks observed near the Fermi level in scanning tunneling spectroscopy dI/dV spectra, along with shifts in the tangential vibrational mode observed in Raman spectra, confirmed n-type and p-type doping effects for the electron-donor peptide/SWCNT and electron-acceptor peptide/SWCNT composites, respectively.

The use of amphiphilic peptides has several significant advantages over other dopants. First, amphiphilic peptides with aromatic side chains are known to produce stable aqueous dispersions of individual SWCNTs.^{20–22} Second, the noncovalent peptide/SWCNT interactions preserve the nanotube's intrinsic structure. Third, solid-phase peptide synthesis is well established, and the functionality of the peptides can be readily controlled by varying the constituent amino acids. Furthermore, peptide-coated SWCNTs can be used as nanoscale biosensors, owing to the biocompatibility and target specific recognition ability of suitably chosen adsorbed peptides.^{21,23,24} One disadvantage of using amphiphilic peptides with a folded secondary structure, such as an α -helix or β -sheet, is their tendency to self-aggregate, which makes them less effective at dispersing SWCNTs.¹⁹ Also, the intermolecular and intramolecular interactions among the peptide moieties may complicate the interpretation of the electronic interaction between the SWCNT and the peptide.

Xie *et al.* reported a new category of designed peptides called surfactant peptides, which essentially have an unordered structure over a large concentration range.²⁵ The current investigation uses surfactant peptides derived from those described by Xie *et al.* because these peptides provide ideal structures to probe peptide/SWCNT electronic interactions. The designed surfactant peptides have a common amino acid sequence of X(Val)₅(Lys)₂, where X indicates phenylalanine or a phenylalanine analog, and Val and Lys indicate valine and lysine residues, respectively (Fig. 1a). The two Lys residues form a polar head at the C-terminus of each peptide, whereas the five Val residues form an apolar tail. The aromatic amino acid (X) at the N-terminus facilitates π – π stacking interactions between the aromatic ring of the amino acid and the SWCNT surface. The incorporation of an aromatic ring at one end of the peptide enables better interaction with the SWCNT surface because the aromatic side chain is less hindered and more flexible than that found in the α -helical peptide system.¹⁹ In addition, compared to α -helices, these short,

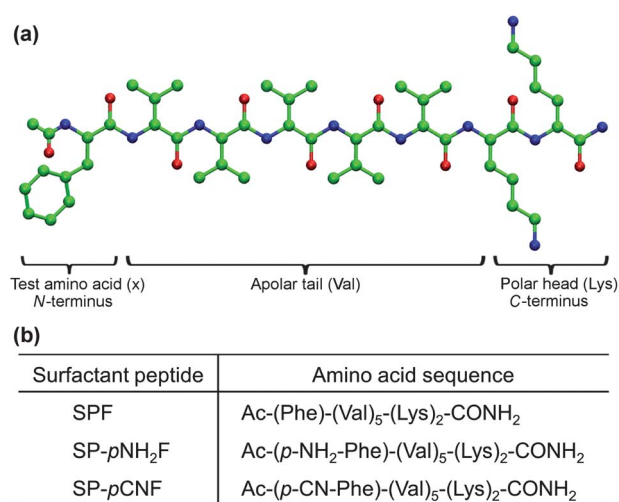


Fig. 1 (a) Schematic representation of a surfactant peptide (atom colors: carbon, green; nitrogen, blue; oxygen, red. Hydrogen atoms are not shown). (b) Amino acid sequences of the three surfactant peptides used in this study. Abbreviations for amino acids: Val → valine, Lys → lysine, Phe → phenylalanine, *p*-NH₂-Phe → *p*-NH₂-phenylalanine, *p*-CN-Phe → *p*-CN-phenylalanine. Ac indicates N-terminal acetylation, and CONH₂ indicates C-terminal amidation.

unordered surfactant peptides are expected to pack more densely on nanotube surfaces.

To investigate the effect of electron-donating or electron-withdrawing functional groups, three surfactant peptides were synthesized by incorporating phenylalanine (Phe) and two phenylalanine analogs, namely *p*-amino-phenylalanine (*p*-NH₂-Phe) and *p*-cyano-phenylalanine (*p*-CN-Phe), as the N-terminal aromatic amino acid. The corresponding amino acid sequences are shown in Fig. 1b. The *p*-NH₂-Phe contains an electron-donating amine group (–NH₂), whereas *p*-CN-Phe contains an electron-withdrawing cyano group (–CN) on the phenyl ring. The two functional groups (amine and cyano) have equal but opposite Hammett sigma constants (–0.66 and 0.66, respectively),²⁶ thereby providing a way to examine any correlation between the doping effect of the two functionalities. The surfactant peptide which contains Phe is used as the reference peptide.

The remainder of the paper is organized as follows. In the first part, the discussion focuses on the preparation of individually dispersed surfactant peptide/SWCNT composites and their characterization using circular dichroism (CD), atomic force microscopy (AFM), and ultraviolet-visible-near-infrared (UV-Vis-NIR) spectroscopy. Subsequently, the effect of the adsorption of the synthesized peptides on SWCNT electronic properties is addressed using Raman spectroscopy and scanning tunneling spectroscopy (STS).

2. Experimental section

2.1 Synthesis of surfactant peptides

Materials: Dichloromethane (99.8%), N-methyl-2-pyrrolidone (99.5%), N,N-dimethylformamide (99.9%), dimethyl sulfoxide (99.9%), N,N-diisopropylethylamine (98+%), pyridine,

trifluoroacetic acid (99%), thioanisole (99%), 1,2-ethanedithiol (98+%), ethyl ether (99.9%), and methanol (99.8%) were purchased from VWR International. Acetic anhydride (97+%) and anisole (99%) were purchased from Fisher Scientific. Piperidine (99%) was purchased from Sigma-Aldrich. *N*-Hydroxybenzotriazole monohydrate (98%), 2-(1*H*-benzotriazole-1-yl)-1,1,3,3-tetramethyluronium hexafluorophosphate (98%), Fmoc-*L*-valine (99+%), and Fmoc-*L*-phenylalanine (99+%) were purchased from SynBioSci Corporation. Fmoc-*N*^z-Boc-*L*-lysine (99%), Fmoc-4[Boc-amino]-*L*-phenylalanine (99%), and Fmoc-4-cyano-*L*-phenylalanine (98+%) were purchased from Chem-Impex International, Inc. ABI-Fmoc-amide resin was purchased from Applied Biosystems. All chemicals were used as received.

Surfactant peptides were synthesized on an Applied Biosystems 433A solid-phase peptide synthesizer, equipped with an Alltech model 450 UV detector, at a 0.1 mmol scale following standard Fmoc (9-fluorenylmethoxycarbonyl) solid-phase peptide synthetic methods.²⁷ The *N*-termini and the *C*-termini of the synthesized surfactant peptides were protected by acetylation and amidation, respectively. Acetylation was carried out by mixing peptide-resin composites with a solution of 9.0 : 0.5 : 0.5 dimethylformamide : acetic anhydride : pyridine. Peptide cleavage was performed using a cocktail consisting of trifluoroacetic acid : thioanisole : ethanedithiol : anisole (9.0 : 0.5 : 0.3 : 0.2), and the resin was removed by filtration. The volume of the filtrate was reduced to 3–5 mL using a stream of nitrogen gas. Finally, crude peptides were precipitated using cold diethyl ether and lyophilized before purification.

2.2 Purification of surfactant peptides

Materials: Acetonitrile (ACN, 99.8%) was purchased from VWR International. Trifluoroacetic acid (TFA, 99.5%) was purchased from Fisher Scientific. All chemicals were used as received.

Purification was performed using a semi-preparative Delta Waters 600 HPLC instrument equipped with a Waters 2487 dual wavelength absorbance detector and a Vydac C4 reversed-phase column (Sorbent Technologies). The crude peptide samples were dissolved in a 10% aqueous acetic acid solution (not more than 15 mg peptide in 1 mL of acetic acid) and injected onto the column. The peptides were purified by gradient elution with 'solvent A', containing 99.9% water and 0.1% TFA, and 'solvent B', containing 90% ACN, 9.9% water, and 0.1% TFA. Sample aliquots were collected and analyzed using matrix-assisted laser desorption-ionization time-of-flight (MALDI-TOF) mass spectrometry to verify their identities (ESI, Table S1†).

2.3 Analysis of the surfactant peptide secondary structure

Surfactant peptide solutions ranging in concentration from 50 to 500 μ M were prepared by diluting stock peptide solutions. The concentrations of the stock solutions were determined by absorption spectroscopy using the extinction coefficients of the chromophores calculated beforehand (ESI, Fig. S1†). CD studies were performed using an Aviv Model 202 circular dichroism spectrometer. All spectra were acquired from 190 to 260 nm at 25 °C using rectangular quartz cuvettes with a 1 mm path length. The wavelength was recorded when the dynode voltage reached

the dynode cutoff of the instrument (500 V). Data acquired beyond the dynode cutoff were not included for calculations. For analysis, the spectra were converted to mean residue molar ellipticity $[\theta]$ using eqn (1), where S_{obs} is the CD signal in milli-degrees, l is the path length of the sample cuvette in cm, c is the concentration of the peptide solution in mol L⁻¹, and n is the number of amino acid residues in the peptide.²⁵ CD spectra of surfactant peptide/SWCNT dispersions were acquired following the same procedure.

$$[\theta] = \frac{S_{\text{obs}}}{10 \times l \times c \times n} \quad (1)$$

2.4 Preparation of surfactant peptide/SWCNT dispersions

Materials: Raw HiPco SWCNTs (lot #R0519) were purchased from Carbon Nanotechnologies Inc.

To prepare dispersions, 1 mL aliquots of the peptide solutions of desired concentrations were added to Eppendorf tubes containing 0.75–1.00 mg of HiPco SWCNTs and vortexed for 1 min. Next, the samples were probe sonicated for 1 min using a VWR Scientific Branson Sonifier 250 at a power level of 10 W, while the samples were immersed in an ice water bath. The sonicated samples were centrifuged at 16 000 $\times g$ for 10 min in an Eppendorf 5417C centrifuge. The upper 75% of the supernatants were transferred to Beckman centrifuge tubes and centrifuged at 20 000 $\times g$ for 15 min in a Beckman TL-100 ultracentrifuge with the temperature controlled at 4 °C. Recovered supernatants were further centrifuged at 50 000 $\times g$ for 30 min and at 100 000 $\times g$ for 1 h. Control samples were prepared following the same procedure excluding SWCNTs.

2.5 Characterization of surfactant peptide/SWCNT dispersions

2.5.1 Determination of SWCNT dispersability by surfactant peptides. **Materials:** Mica substrates (1/4" \times 1/4" \times 0.008/0.010") were purchased from Asheville-Schoonmaker Mica Co. Silicon cantilevers (model#: MPP-12100-100) were purchased from Veeco Probes.

A Perkin-Elmer Lambda 900 UV-Vis-NIR spectrophotometer was used to acquire absorption spectra of the surfactant peptide/SWCNT dispersions collected after the 100 000 $\times g$ spin. Spectra were collected from 400 to 1400 nm using rectangular quartz cuvettes with a 1 mm path length. Nanopure water was used as the blank sample.

AFM imaging was performed under ambient conditions using a Digital Instruments, Inc. Nanoscope III Multimode Scanning Probe Microscope operated in the TappingMode™. To isolate the AFM from mechanical vibrations, imaging was performed on a vibration isolation table (MICRO-g® 63-561, Technical Manufacturing Corporation). For image acquisition, silicon cantilevers with a force constant of 5 Nm⁻¹ and an average resonance frequency of 150 kHz were used. Before image acquisition, the 'J' scanner was calibrated in the x , y and z dimensions using a standard sample (NanoDevices Inc.) containing lines with a 2 μ m pitch and 20 nm height. The height (z) calibration was verified using hydrofluoric acid etched pits in muscovite mica, in which 2 nm steps are observed along the long

axis and 1 nm steps are observed along the short axis. For the AFM analysis of peptide-coated SWCNTs, the dispersions were diluted 20-fold with nanopure water, and 10 μL volumes of these dispersions were drop-cast onto freshly cleaved mica substrates and dried in a desiccator for 24 h before imaging. Control samples were prepared by following the same procedure using solutions containing only surfactant peptides. In addition, 20 μL volumes of 1,2-DCE/SWCNT supernatants were spun-cast (3500 rpm, 30 s) onto freshly cleaved mica substrates and dried in a desiccator for the AFM analysis of bare SWCNTs.

2.5.2 Investigation of the effect of surfactant peptides on SWCNT electronic properties. *Materials:* A SpectRimTM substrate was purchased from Tienta Sciences, Inc. Highly oriented pyrolytic graphite (HOPG) substrates were purchased from GE Advanced Ceramics. Au(111)-coated mica substrates were purchased from Agilent Technologies, Inc. STM probes (8 mm cut Pt/It wire, model: PT) were purchased from Veeco Probes.

Raman spectra were acquired using a Jobin Yvon Horiba high-resolution LabRam Raman microscope system equipped with a Spectra-Physics Model 127 helium–neon laser (632.8 nm excitation, 8 mW power) and a SynapseTM CCD detector. Peptide/SWCNT dispersions (100 000 \times g) were spotted on a SpectRimTM substrate and dried before analysis. To obtain a better signal-to-noise ratio, multiple ~ 1 μL aliquots of sample were applied to obtain the desired spot concentration. When acquiring spectra, the laser was focused to a spot of ~ 1 μm using a 50 \times objective and 350 μm slit. Wavenumber calibration was carried out using a silicon wafer (520.5 cm^{-1}). Raman spectra were acquired from 50 to 3000 cm^{-1} with a total acquisition time of 5 min. The spectra were fitted with Lorentzian functions using LabSpec version 5.24.19 software.

For STM/STS analysis, 20 μL volumes of peptide/SWCNT supernatants (100 000 \times g) and 1,2-DCE/SWCNT supernatants were spun-cast onto Au(111)-coated mica substrates at a speed of 3500 rpm for 30 s and dried in a desiccator for 24 h prior to imaging. Control samples were prepared by following the same procedure using solutions containing only surfactant peptides. STM analysis was done at room temperature under ambient conditions using a Digital Instruments, Inc. Nanoscope III STM equipped with a 0.7 μm 'A' scanner and Pt/Ir tips. To isolate mechanical vibrations, the microscope was placed on a gel pad on a cement block suspended from a tripod with bungee cords. Also, the STM instrument was covered with a neoprene hood to reduce any effect from acoustic noise. Before data acquisition, the scanner was calibrated using HOPG to ensure the accuracy of the measurements. When imaging SWCNTs, large scan sizes (100–200 nm) were initially viewed using constant current mode to verify that the analysis was done on a fairly flat region. After locating SWCNTs, the scan size was reduced to approximately 10 to 20 nm, and the images were acquired in the constant height mode.

To acquire a scanning tunneling spectrum from a certain position on a nanotube, the feature of interest was brought to the center of the image and the microscope was switched to the STS mode. The I - V data were collected with the feedback loop switched off, and the current (I) was recorded as a function of bias voltage (-1.0 to 1.0 V). Twenty I - V curves were collected

and averaged to increase the signal-to-noise ratio. The I - V data were converted to differential tunneling conductance (dI/dV) and plotted against the bias voltage. The resulting curves were Fourier filtered to further reduce the noise. STM images and corresponding STS I - V curves were acquired from HOPG substrates to verify the accuracy of data acquisition. Reference measurements were also performed on bare regions of the Au(111) substrates. STS spectra were acquired from the surfactant peptide control samples following the same method.

3. Results and discussion

3.1 Structural behavior of surfactant peptides in the absence and presence of SWCNTs

Surfactant peptides, as revealed in the literature, have primarily a random coil structure presumably due to their low molecular weight and arrangement of amino acids.²⁵ Owing to the lack of secondary structure, formation of inter- and intramolecular folding interactions among the surfactant peptide moieties is minimal. Circular dichroism is an excellent technique to characterize the structural behavior of peptides in solution. The arrangement of the peptide backbone amide bonds, which gives rise to characteristic spectral features, allows the identification of different structural conformations present in a sample.²⁸ Fig. 2 shows the CD spectra of the synthesized surfactant peptides, SPF, SP- $p\text{NH}_2\text{F}$, and SP- $p\text{CNF}$, in both the absence and presence of SWCNTs. As presumed, CD spectra of the samples containing only surfactant peptides show similar spectral features over the studied concentration range (50–500 μM), suggesting the absence of concentration-induced structural changes (Fig. 2a–c). The strong negative feature around 200 nm indicates that the majority of the surfactant peptide molecules exist as random coils in solution.^{25,28} This behavior is distinct from long chain peptides, such as the 29 residue nano-1, which tend to form secondary conformations (α -helical for nano-1) at high concentrations as well as when adsorbed onto SWCNT surfaces.²²

To examine the structural behavior of the synthesized surfactant peptides in the presence of SWCNTs, CD spectra were acquired from surfactant peptide/SWCNT dispersions (Fig. 2d–f). In these samples, surfactant peptide molecules adsorbed onto the SWCNT surfaces, as well as those that remain in the solution, contribute to the CD signal. Similar to the samples containing only surfactant peptides, these spectra, except those acquired from the 100 μM SPF/SWCNT and SP- $p\text{CNF}$ /SWCNT dispersions which have intensities too small for meaningful interpretation, show a strong peak around 200 nm and a less prominent feature around 220 nm. This result confirms that, unlike the helical peptides, the surfactant peptides maintain their random coil structure even in the presence of SWCNTs. The CD spectra obtained from the surfactant peptide/SWCNT dispersions exhibit significant variations in the signal intensity. Unlike the surfactant peptide solutions, the peptide/SWCNT dispersions were centrifuged in order to remove SWCNT bundles and other impurities present in the samples. It is likely that some surfactant peptide adsorbed onto SWCNTs and SWCNT bundles was removed from the supernatant during this process diminishing the overall CD signal.

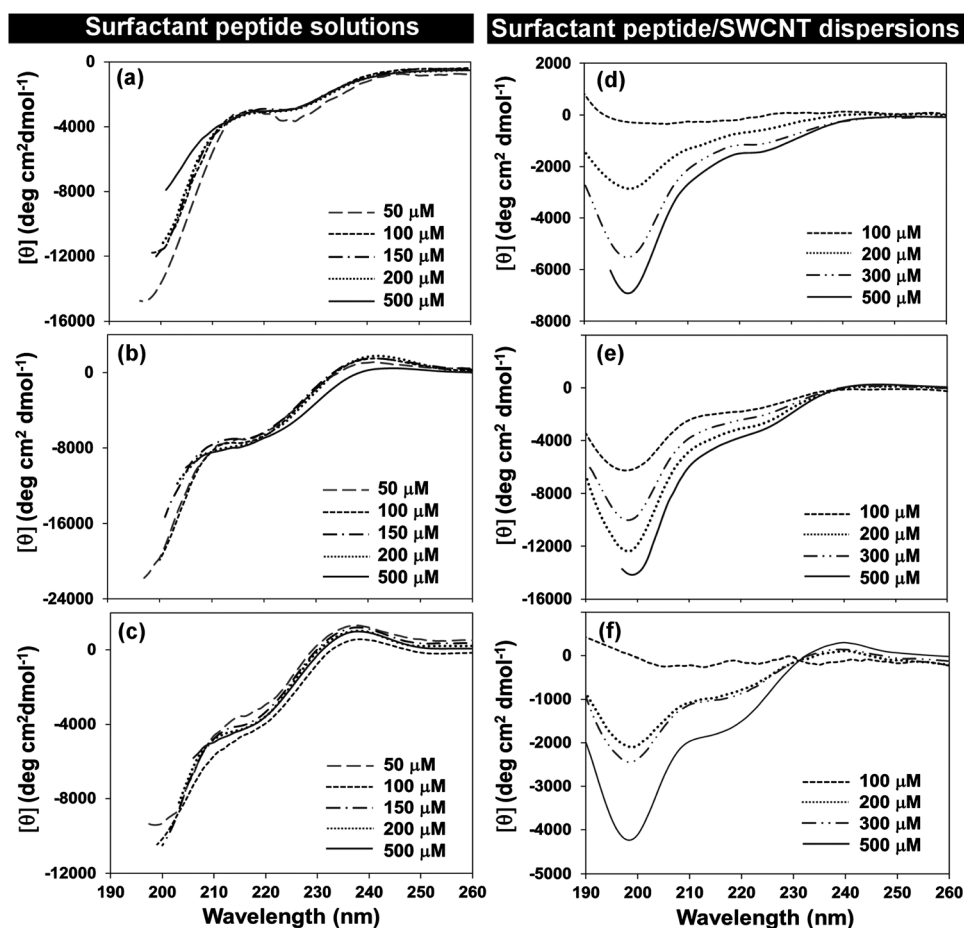


Fig. 2 Left column: CD spectra of surfactant peptides: (a) SPF, (b) SP-*p*NH₂F, and (c) SP-*p*CNF. Right column: CD spectra of surfactant peptide/SWCNT dispersions: (d) SPF/SWCNT, (e) SP-*p*NH₂F/SWCNT, and (f) SP-*p*CNF/SWCNT. $[\theta]$ indicates mean residue molar ellipticity. CD data were not reported beyond a dynode cutoff voltage of 500 V. Different samples reached the dynode cutoff at different wavelengths.

The CD spectra of the surfactant peptide/SWCNT dispersions, especially SP-*p*NH₂F/SWCNT (Fig. 2e) and SP-*p*CNF/SWCNT (Fig. 2f), indicate the presence of an isodichroic point in the region of 230–240 nm. In CD spectroscopy, an isodichroic point suggests conversion between two distinct states or species in solution.²⁸ However, in the current experiment, the CD spectra do not indicate a significant transition from one structure to another since all spectra display random coil behavior at all concentrations. Hence, the isodichroic point may suggest a change in the arrangement of surfactant peptides on SWCNT surfaces at higher concentrations.²⁹ For example, at low concentrations, peptide molecules may be disordered on nanotube surfaces, whereas at higher concentrations, peptide molecules should be more crowded and gain more order as they self-organize to densely coat the SWCNT surface.

3.2 SWCNT dispersability by surfactant peptides

Prior to investigating the effect of surfactant peptides on SWCNT electronic properties, the dispersability of SWCNTs in the surfactant peptide solutions was examined using AFM and UV-Vis-NIR spectroscopy. Based on the preliminary AFM data (ESI, Fig. S2 and S3†), 500 μM surfactant peptide solutions collected after the 100 000 × *g* centrifugation step were

chosen to carry out further experiments. AFM images shown in Fig. 3a–c exhibit well-dispersed SWCNTs and clean backgrounds with little particulate matter or excess peptide, and hence are useful for AFM diameter analysis of the SWCNTs. Control AFM studies were performed using solutions containing only surfactant peptides, which were prepared following the same procedure used for peptide/SWCNTs (exclusive of SWCNTs). Shown in Fig. 3d–f are the corresponding AFM images of the peptide control samples. These images confirm that the surfactant peptides alone do not form nanotube-like features.

AFM height measurements have been used previously to determine the diameters of peptide-coated SWCNTs.^{30–32} For example, the average diameter of SWCNTs coated with α -helical nano-1 peptide was reported as 2.4 ± 1.3 nm,³¹ whereas the average diameters of SWCNTs coated with reversible cyclic peptides, RC5 and RC7, were 1.45 ± 0.22 nm and 1.73 ± 0.30 nm, respectively.³² To verify the presence of individual SWCNTs in the surfactant peptide/SWCNT dispersions, AFM height measurements were obtained from bare regions of the SWCNTs. The average SWCNT diameter and the standard deviation of each measurement set are: SPF/SWCNT = 0.80 ± 0.13 nm (number of SWCNTs (*n*) = 35), SP-*p*NH₂F/SWCNT = 0.76 ± 0.11 nm (*n* = 30), and SP-*p*CNF/SWCNT = 0.79 ± 0.09

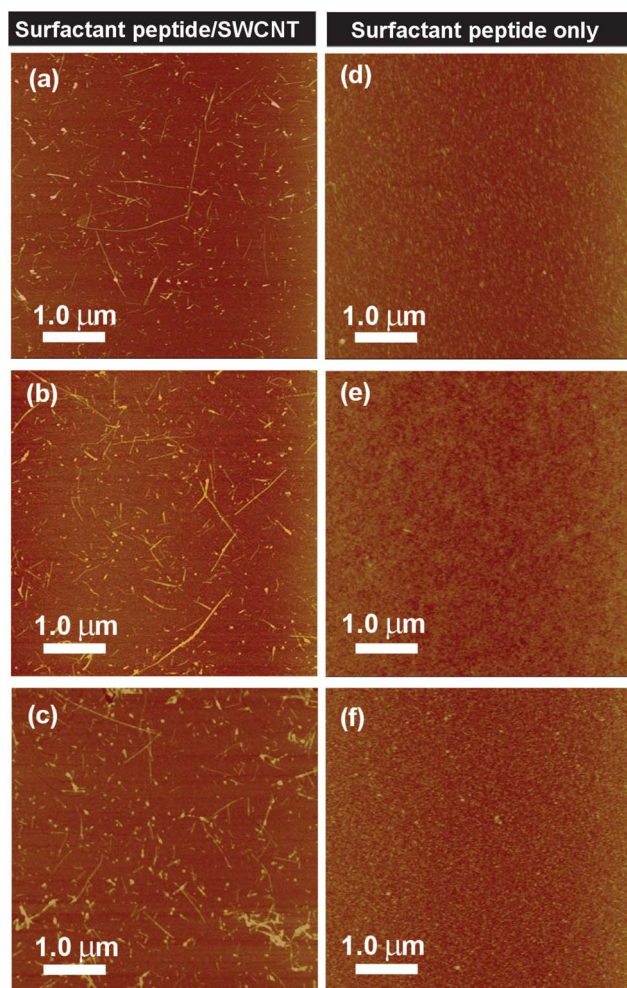


Fig. 3 Left column: AFM images ($5.0 \times 5.0 \mu\text{m}$) of 20-fold diluted 500 μM (a) SPF/SWCNT, (b) SP-*p*NH₂F/SWCNT, and (c) SP-*p*CNF/SWCNT dispersions. Right column: AFM images ($5.0 \times 5.0 \mu\text{m}$) of 20-fold diluted 500 μM (d) SPF, (e) SP-*p*NH₂F, and (f) SP-*p*CNF peptide solutions (exclusive of SWCNTs).

nm ($n = 30$). The reported diameter range for HiPco SWCNTs is from 0.7 to 1.4 nm.³³ Accordingly, the measured diameters confirm the presence of individually dispersed nanotubes in the surfactant peptide/SWCNT dispersions. AFM height measurements were also taken from the peptide-coated regions of the SWCNTs. The resultant data reveal that the average thickness of the surfactant peptide coating is about 1 nm (e.g., SPF 1.12 ± 0.53 nm, SP-*p*NH₂F 0.96 ± 0.49 nm, and SP-*p*CNF 1.00 ± 0.43 nm). Based on the dimensions of a single peptide backbone,³² it can be speculated that, in most cases, there is a single layer of peptide lying parallel to the SWCNT surface. Having singly dispersed SWCNTs with a thin peptide coating is vital for the scanning tunneling microscopy and scanning tunneling spectroscopy studies. As compared to the other peptide/SWCNT systems,^{31,32} the surfactant peptide/SWCNT system contained nanotubes with smaller diameters. This narrow diameter range may have resulted from the high centrifugation speed ($100\,000 \times g$) used during the preparation of the dispersions. Another possible reason could be the preference of the peptides to disperse SWCNTs with smaller diameters.

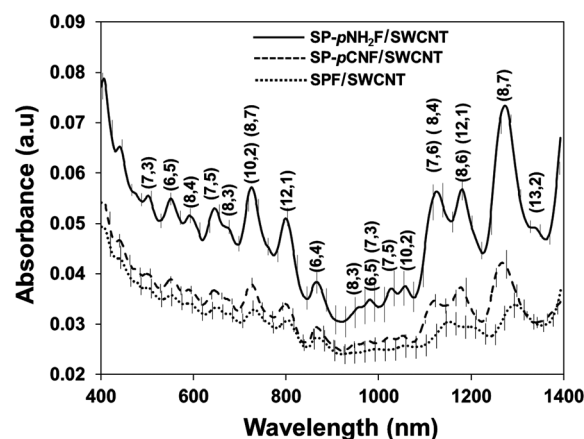


Fig. 4 Average UV-Vis-NIR spectra ($n = 3$) of 500 μM surfactant peptide/SWCNT dispersions collected after the $100\,000 \times g$ spin. Vertical lines show standard deviations for each sample. Numbers in the parentheses represent assigned (n,m) chiralities.

The absorption spectra of the 500 μM surfactant peptide/SWCNT dispersions ($100\,000 \times g$) are shown in Fig. 4. To ensure reproducibility, three dispersions of each peptide/SWCNT composite were analyzed using the same experimental conditions, and the resultant spectra were averaged. The vertical lines in each spectrum show the standard deviations of the absorbance reading. In general, UV-Vis-NIR spectra of SWCNTs are characterized by a series of relatively strong peaks resulting from electronic transitions between the van Hove singularities in their electronic density of states.³⁴ Well-defined spectral features are indicative of debundled carbon nanotubes.³⁵ As can be seen in Fig. 4, all the spectra are comprised of characteristic absorption features, confirming the presence of SWCNTs in the samples. The absorption spectrum of SP-*p*NH₂F/SWCNT shows the most pronounced peaks, suggesting that this peptide is more effective in dispersing SWCNTs than the other two peptides. This behavior is consistently observed in all absorption spectra acquired from the surfactant peptide/SWCNT dispersions spun at different centrifugation speeds (ESI, Fig. S4†). It is also observed that the absorption of SP-*p*CNF/SWCNT is slightly higher than that of SPF/SWCNT. This observation is consistent with previous data showing that aromatic rings with functional groups exhibit better adsorption onto SWCNT surfaces than unsubstituted aromatic rings.³⁶ Hence, the presence of an amine or a cyano group presumably lead to a more efficient adsorption of SP-*p*NH₂F and SP-*p*CNF on SWCNTs compared to SPF.

The peak positions in the absorption spectra can be used to identify the different chiralities and associated (n,m) indices of SWCNTs present in the samples.^{37,38} The numbers shown in parentheses in Fig. 4 are the assigned SWCNT chiralities obtained from the surfactant peptide/SWCNT dispersions based on similarities to SDS-dispersed SWCNTs.³⁷ The peak fitting data of the spectra are listed in ESI, Table S2†. These data clearly show that the peaks in the region of ~ 400 to 900 nm are almost completely overlapping, in contrast to some peaks in the region of ~ 900 to 1300 nm, wherein significant peak shifting is evident. This behavior is commonly reported in the literature.^{39,41} In general, the existence of SWCNT bundles cause red shifting of the peaks as

compared to singly dispersed SWCNTs.³⁹ Moreover, absorption peak shifting occurs in the presence of different dielectric environments near SWCNTs.⁴⁰ Most of the absorption peaks observed in the 900–1300 nm region for SP-*p*NH₂F/SWCNT and SP-*p*CNF/SWCNT composites show a blue-shift as compared to those observed for SPF/SWCNT. This may result from the different dielectric environments created by the peptides themselves due to the presence of electron-donating or electron-withdrawing groups on their aromatic ring. However, at present, it is not well understood why both SP-*p*NH₂F/SWCNT and SP-*p*CNF/SWCNT composites show a blue shift as compared to the reference.

3.3 Investigation of SWCNT electronic properties

To attain a better understanding of the effect of surfactant peptides on SWCNT electronic properties, Raman spectroscopy was performed on the peptide/SWCNT dispersions. Important features in the Raman spectrum of SWCNTs include the radial breathing mode (RBM, 100–300 cm⁻¹), disorder-induced band (D-band, 1250–1450 cm⁻¹), tangential band (G-band, 1500–1600 cm⁻¹), and the second overtone of the D-band (G'-band, 2500–2900 cm⁻¹).⁴² The frequency position of the Raman G-band peak is often used to probe the effect of dopants on SWCNT and graphene electronic properties.^{8,10,12,16,17,19,43–45} Generally, a downshift of the G-band peak frequency indicates charge transfer from the dopant to the carbon nanotube, suggesting an n-type doping effect,^{8,10,12,17,19,43,44} whereas an upshift reveals charge transfer from the carbon nanotube to the dopant, signifying a p-type doping effect.^{8,10,12,16,19,43,45}

Fig. 5a presents Raman spectra of surfactant peptide-coated SWCNT composites. To test the effect of the amine (electron-donating) and cyano (electron-withdrawing) functional groups on the peptide/SWCNT interaction, the G-band peak positions of the SP-*p*NH₂F/SWCNT and SP-*p*CNF/SWCNT composites were compared to that of the reference SPF/SWCNT composite (Fig. 5b). As indicated in the figure, a downshift of the G-band peak is evident for SP-*p*NH₂F/SWCNT, while an upshift is observed for the SP-*p*CNF/SWCNT composite. To verify this trend, Raman spectra were acquired from three separately prepared dispersions of each composite, all on the same day. Two additional trials were performed on one of the sets of dispersions.

The average G-band peak positions and the standard deviations calculated from these five trials are: SPF/SWCNT = 1591.7 ± 0.1 cm⁻¹, SP-*p*NH₂F/SWCNT = 1589.9 ± 0.3 cm⁻¹, and SP-*p*CNF/SWCNT = 1592.9 ± 0.1 cm⁻¹. Reproducible G-band peak values were obtained from different sets of dispersions, confirming that the observed shifts are not caused from errors associated with the experimental conditions or procedures (ESI, Table S3†). Compared to the G-band peak value for SPF/SWCNT, the average downshift observed for the SP-*p*NH₂F/SWCNT composite is -1.8 ± 0.3 cm⁻¹ and the average upshift observed for SP-*p*CNF-coated SWCNTs is 1.2 ± 0.1 cm⁻¹. The observed downshift indicates charge transfer from the surfactant peptide to the SWCNT (n-type behavior), correlating well with the strong electron-donating ability of the amine group on the phenyl ring of the peptide. On the other hand, the upshift observed in the G-band peak frequency suggests charge transfer from the SWCNT to the surfactant peptide, suggesting a p-type doping effect. This result is consistent with the presence of the strong electron-withdrawing cyano group on the aromatic ring of the peptide.

A similar shifting pattern in the Raman tangential band was observed for SWCNTs coated with α -helical peptides containing aromatic amino acids bearing electron-donating hydroxyl (tyrosine) and electron-withdrawing nitro groups (*p*-nitro-phenylalanine).¹⁹ These two peptides were identified as Tyr-nano-1 and nitro-nano-1, respectively. Even though the directions of the G-band peak shifts of the surfactant peptide-coated SWCNTs are similar to those observed for α -helical peptide-coated SWCNTs, there is a considerable difference in the magnitudes of the shifts. Specifically, the downshift observed for the SP-*p*NH₂F/SWCNT composite (-1.8 ± 0.3 cm⁻¹) is nearly 3-fold greater than that observed for Tyr-nano-1/SWCNT (-0.6 ± 0.2 cm⁻¹), while the upshift observed for SP-*p*CNF/SWCNT (1.2 ± 0.1 cm⁻¹) is nearly double that of nitro-nano-1/SWCNT (0.7 ± 0.3 cm⁻¹). This implies that the studied surfactant peptides are more effective in doping SWCNTs than the α -helical peptide/SWCNT systems reported, since it has been revealed that the magnitude of the G-band peak shifting correlates with the degree of doping.^{43,44}

The doping effect of the surfactant peptides on SWCNTs was further examined using scanning tunneling microscopy (STM) and scanning tunneling spectroscopy (STS). STM is widely used to obtain structural images of carbon nanotubes with atomic

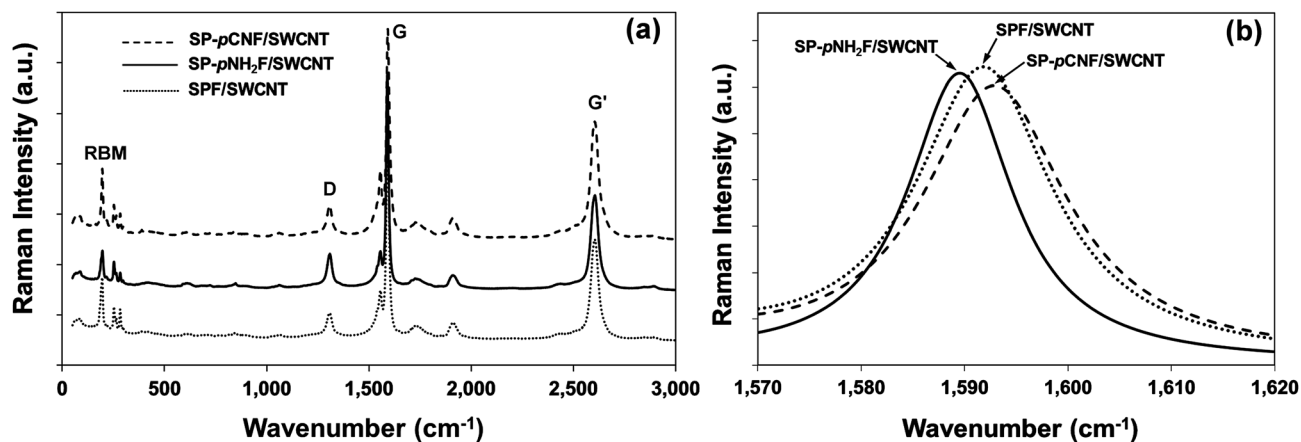


Fig. 5 (a) Raman spectra of surfactant peptide/SWCNT dispersions. (b) Raman G-band peak region.

resolution, while STS is employed to investigate the local electronic density of states (LDOS) of the material.^{46–48} To examine electronic properties, local I - V curves obtained from samples are numerically converted to the equivalent differential conductance (dI/dV) spectra, which are proportional to the LDOS of materials.^{47,49}

Prior to STM/STS studies of the SWCNTs, analyses were carried out on the HOPG and Au(111)-coated mica substrates. The STS I - V curves of these two reference substrates correlate well with data reported in literature (ESI, Fig. S5†).^{50,51} To ensure the accuracy of data acquisition, STM images and corresponding STS I - V curves were acquired from freshly cleaved HOPG substrates prior to all STM/STS analyses of peptide/SWCNT samples. The STS dI/dV spectra of the peptide controls are virtually featureless, demonstrating that peptide contributions to the density of states in the bias range of -1.0 to 1.0 V are minimal (ESI, Fig. S6†).

Due to the 1-dimensional nature of carbon nanotubes, the LDOS of metallic and semiconducting SWCNTs are split into several sub-bands (van Hove singularities) and exist as well-defined sharp features that can be observed in STS differential conductance (dI/dV) or normalized conductance ($[I/V][dI/dV]$) spectra.^{46,47,49} The LDOS at the Fermi level also indicate whether the SWCNT is semiconducting or metallic.⁴⁷ Fig. 6 presents a STM image (Fig. 6a) and STS dI/dV spectra (Fig. 6b and c) obtained from uncoated SWCNTs that were dispersed using 1,2-dichloroethane (ESI, Fig. S7†). The STM image of the uncoated SWCNT clearly shows the atomic structure of the carbon lattice. The average distance measured between bright points in the image was 0.26 nm, which correlates well with the lattice spacing reported for graphene sheets.⁵² The dI/dV spectrum in Fig. 6b exhibits very low LDOS near the Fermi level along with strong increases in the electronic states away from the Fermi level, confirming its semiconducting behavior. In contrast, the increased LDOS at the Fermi level of the dI/dV spectrum for a different SWCNT, shown in Fig. 6c, verifies metallic behavior. In this study, much attention is given to the electronic structure of semiconducting SWCNTs.

The dI/dV spectra acquired sequentially at a single position on an uncoated semiconducting SWCNT and the spectra acquired from different positions on the same uncoated SWCNT are shown in Fig. 7a and b, respectively. All spectra show similar features, confirming the reproducibility of data acquisition. Unlike the

sharp singularities predicted by theory, the observed LDOS are somewhat broader and less well-pronounced, possibly due to hybridization between the wavefunctions of the SWCNT and the gold substrate, which is a common phenomenon reported in STS.⁴⁹ To further analyze the electronic structure of uncoated SWCNTs, STS dI/dV spectra were acquired from 17 uncoated SWCNTs (data not shown) in which 76% show semiconducting characteristics, while 24% of the SWCNTs show characteristics of metallic SWCNTs. The measured semiconducting-to-metallic ratio is comparable to the reported 3 : 1 ratio for HiPco SWCNTs.⁵³

STM images of the surfactant peptide-coated SWCNTs are presented in Fig. 8. In contrast to uncoated SWCNTs, the atomic

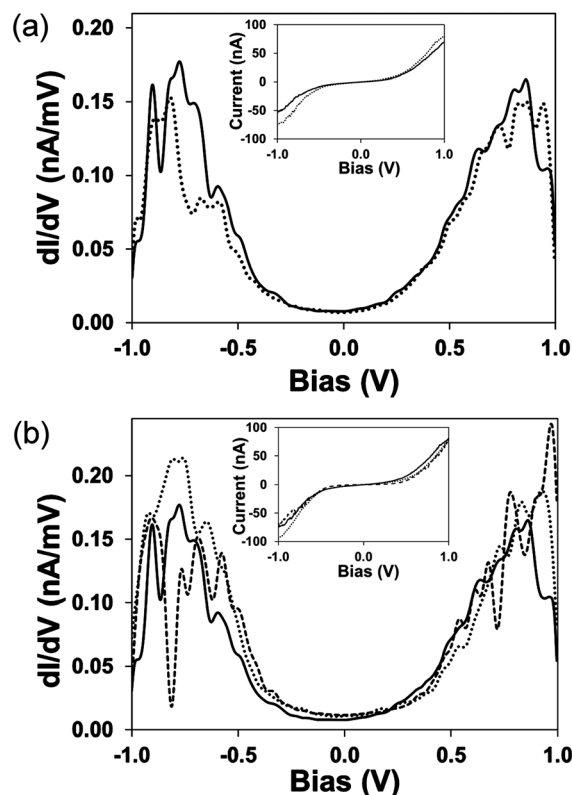


Fig. 7 STS dI/dV spectra acquired from an uncoated SWCNT. (a) Spectra taken sequentially at the same location, and (b) spectra taken at different locations. The insets show the corresponding I - V curves.

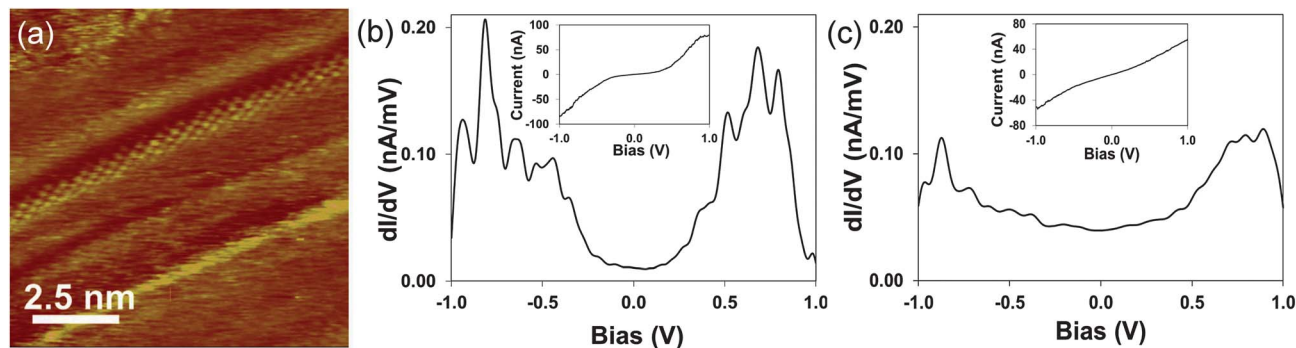


Fig. 6 (a) STM image of an uncoated SWCNT on a Au(111)-coated mica substrate. (b) STS dI/dV spectrum of an uncoated SWCNT showing semiconducting behavior. (c) STS dI/dV spectrum of an uncoated SWCNT showing metallic behavior.

structure of the carbon lattice is not observed for peptide-coated SWCNTs because the low intrinsic conductivity of the peptide obscures the atomic structure of the SWCNT.¹⁹ The presence of a thin layer of peptide on most nanotubes was verified previously by the AFM height images and the section analysis of the bare regions and the peptide-coated regions of the SWCNTs. For STS studies of SWCNTs, it is important to minimize SWCNT bundling as well as thick peptide coatings on nanotube surfaces, as both of these factors have a negative effect on the analysis. For example, the inter-tube interactions cause alterations of the SWCNT electronic density of states.^{46,48} Also, since the tunneling current decays exponentially with the tip-sample distance, a thick layer of low conductivity peptide on SWCNTs could presumably act as a barrier for electron tunneling.¹⁹

Fig. 9 shows a comparison of the LDOS of the three surfactant peptide-coated SWCNT systems, namely SPF/SWCNTs (Fig. 9a), SP-*p*NH₂F/SWCNTs (Fig. 9b), and SP-*p*CNF/SWCNTs (Fig. 9c). Since STS accounts for the local density of states, the consequential changes that occur in the electronic structure of SWCNTs, especially due to doping, can successfully be observed by studying the tunneling spectra.^{7,14,19,54} Specifically, for n-doped carbon nanotubes, an additional “donor-like” feature is present in the DOS above the Fermi level on the conduction band side,^{19,54,55} whereas for p-doped carbon nanotubes, an additional “acceptor-like” feature appears below the Fermi level on the valence band side.^{14,19,55} According to theoretical and experimental observations, these new features appear fairly close to the Fermi level, typically within the range of -0.20 to 0.20 V.^{14,19,54,55}

The STS dI/dV spectrum acquired from a SPF-coated SWCNT (Fig. 9a) show symmetrically placed LDOS on either side of the Fermi level. The vanishing LDOS at the Fermi level of the dI/dV spectrum and the rectifying behavior of the $I-V$ curve

(Fig. 9a inset) suggest a semiconducting SWCNT. A total of 14 SWCNTs coated with SPF were studied with STS, and 86% are identified as semiconducting SWCNTs, whereas 14% are identified as metallic SWCNTs. The STS dI/dV spectra obtained for SPF/SWCNT composites closely resemble those acquired for uncoated SWCNTs (Fig. 7), suggesting that the electronic properties of SWCNTs coated with SPF are not noticeably altered by this peptide. Since the Phe residue of SPF does not have a donor or acceptor functional group on the aromatic ring, significant modifications to the dI/dV spectrum are not expected.

A STS dI/dV spectrum of a semiconducting SWCNT coated with SP-*p*NH₂F is shown in Fig. 9b. The first van Hove singularity peaks at around ± 0.30 V are fairly symmetrically placed about the Fermi level. However, unlike the uncoated and SPF-coated SWCNTs, the dI/dV spectrum of SP-*p*NH₂F/SWCNT shows an extra peak on the conduction band side close to the Fermi level, at around 0.20 V. This peak is similar to those observed for n-doped materials.^{19,54,55} To further observe this behavior, STS spectra were acquired from 36 SWCNTs coated with SP-*p*NH₂F, wherein 78% show semiconducting and 22% show metallic characteristics. For the semiconducting SWCNTs, 43% show an extra peak only in the conduction band region close to the Fermi level as shown in Fig. 9b. The bias voltages associated with peaks observed within the -0.20 to 0.20 V range were measured and are listed in the ESI, Table S4-c†. In some spectra, two small symmetric peaks are observed closer to the Fermi level (within the -0.2 to 0.2 V range) on both the conduction and valence band sides. These arise presumably due to defect sites or inherent deformations of the SWCNTs.^{56,57}

Fig. 9c presents a STS dI/dV spectrum obtained from a SP-*p*CNF-coated semiconducting SWCNT. In contrast to the SP-*p*NH₂F-coated SWCNT (Fig. 9b), an additional feature for the SP-*p*CNF-coated SWCNT appears on the valence band side at

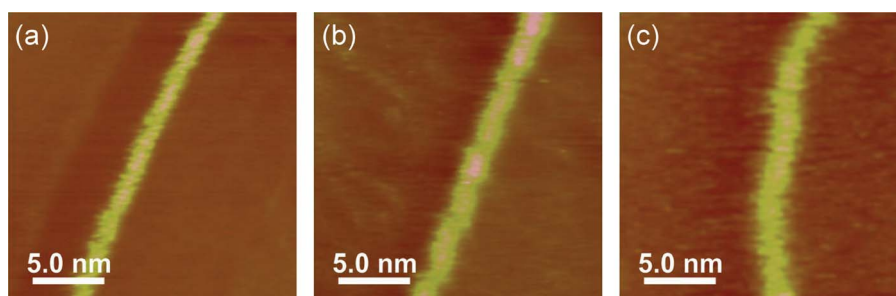


Fig. 8 STM images of (a) SPF/SWCNT, (b) SP-*p*NH₂F/SWCNT, and (c) SP-*p*CNF/SWCNT on Au(111)-coated mica substrates.

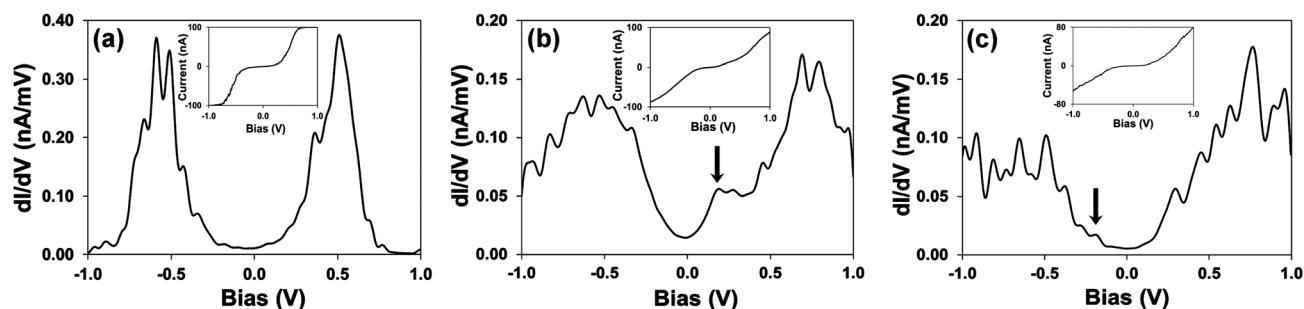


Fig. 9 STS dI/dV spectra of (a) SPF/SWCNT, (b) SP-*p*NH₂F/SWCNT, and (c) SP-*p*CNF/SWCNT. The insets show the corresponding $I-V$ curves. Arrows in (b) and (c) indicate the additional peaks in the conduction band and the valence band, respectively.

around -0.19 V, which is similar to those observed for p-doped materials.^{19,55} Further analysis was performed on 34 SWCNTs coated with SP-*p*CNF. The STS I - V and dI/dV spectra reveal that 88% of these tubes are semiconducting, while 12% are metallic. The bias voltages associated with the peaks observed within the -0.20 to 0.20 V region of the dI/dV spectra of semiconducting tubes are summarized in Table S4-d in the ESI†. Apart from the SWCNT composites that do not show any features in this region, as well as those that show features on both sides, 30% exhibit additional features on the valence band side indicating a p-doping effect. Both SP-*p*NH₂F/SWCNT and SP-*p*CNF/SWCNT composites show low percentages of doped SWCNTs (43% and 30%, respectively). This result may suggest that a fraction of the SWCNTs examined do not have sufficient peptide coverage to cause a measurable doping effect. Since STS measurements are localized, the dI/dV spectra obtained from such areas may reflect unperturbed electronic structure. SWCNTs with a greater peptide coverage could have been used for the experiment, however, a thick peptide layer could inhibit electron tunneling.

When comparing the STS dI/dV spectra of the SP-*p*NH₂F and SP-*p*CNF surfactant peptide/SWCNT composites, it is evident that the extra peaks observed for SP-*p*NH₂F/SWCNT are more prominent than those of SP-*p*CNF/SWCNT. Even though the amine and cyano groups have equal but opposite Hammett sigma constants, STS, Raman, and absorption spectroscopy observations of the three composites lead to the conclusion that SP-*p*NH₂F is much more successful in altering SWCNT electronic properties than SP-*p*CNF. The greater ability of the SP-*p*NH₂F peptide to disperse SWCNTs, which is primarily observed from the pronounced absorption peaks in the UV-Vis-NIR spectra of the SP-*p*NH₂F/SWCNT dispersions (Fig. 4), suggests better packing of this peptide on SWCNTs, wherein the aromatic rings are favorably oriented to π -stack with the nanotube surface to cause an effective donor-acceptor interaction.

The STS dI/dV results reported for SWCNTs coated with α -helical peptides containing tyrosine (Tyr-nano-1) and *p*-nitro-Phe (nitro-nano-1) showed similar behavior.¹⁹ However, the additional peaks observed for the surfactant system are more pronounced than those observed for the α -helical system. The difference in the peptide structure may cause the disparity between the two systems. For example, the simple structure of the surfactant peptide allows it to orient favorably and pack more densely on a SWCNT surface as compared to an α -helical peptide, resulting in a higher aromatic concentration on the nanotube surface. Apart from this, the presence of different electron-donating and electron-withdrawing functional groups on the interacting amino acids may also have an effect on π - π stacking interactions between the peptides and the SWCNTs. The strong electron-donating ability of the amine group on *p*-amino-Phe (Hammett $\sigma = -0.66$) as compared to the hydroxyl group on tyrosine (Hammett $\sigma = -0.37$) presumably leads to the enhanced perturbation of SWCNT electronic properties. Despite the stronger electron-withdrawing ability of the nitro group (Hammett $\sigma = 0.78$) vs. the cyano group (Hammett $\sigma = 0.66$), SWCNTs coated with SP-*p*CNF show prominent additional peaks on the valence band side, verifying that the surfactant peptides used in the current study are more effective in modifying SWCNT electronic properties than the α -helical peptide/SWCNT systems.

4. Conclusions

We found that the designed surfactant peptides containing aromatic amino acids with electron-donating (SP-*p*NH₂F) or electron-withdrawing (SP-*p*CNF) functional groups can be used to modify the electronic properties of SWCNTs by adsorbing them onto SWCNT surfaces. The presence of a donor-acceptor functional group caused changes in the electron density of the peptide aromatic ring, resulting in significant alterations of SWCNT electronic structure. This was demonstrated by comparing the properties of surfactant peptide/SWCNT composites generated using SP-*p*NH₂F and SP-*p*CNF with an SPF/SWCNT composite. CD analyses performed on the surfactant peptides, both in the absence and presence of SWCNTs, revealed random coil structures that were independent of concentration within the range studied. Hence, the observed effects of the surfactant peptides on SWCNTs presumably resulted from the different functionalities within the peptides. AFM images of the surfactant peptide/SWCNT composites showed well-dispersed SWCNTs with clean backgrounds, which were essential for STM/STS analysis. Diameter analysis carried out on the bare regions of the SWCNTs verified the presence of individually dispersed SWCNTs. UV-Vis-NIR absorption data revealed that SP-*p*NH₂F is far more effective in dispersing SWCNTs in solution than the other two peptides. The absorption peak shifts observed in the region of 900–1300 nm indicated the presence of different dielectric environments among the surfactant peptide/SWCNT composites.

The Raman G-band downshift of the SP-*p*NH₂F/SWCNT composite (-1.8 ± 0.3 cm⁻¹) and the peak upshift of the SP-*p*CNF/SWCNT composite (1.2 ± 0.1 cm⁻¹), with respect to SPF/SWCNT, provided evidence for a charge transfer interaction between the peptides and the SWCNTs. Specifically, the downshift of the G-band indicated an n-doping effect, while the upshift indicated a p-doping effect. The additional features observed in the STS dI/dV spectra further confirmed the ability to dope SWCNTs with SP-*p*NH₂F and SP-*p*CNF peptides. Similar to bare SWCNTs, the symmetrically positioned LDOS of the SPF/SWCNT composite suggested that a donor-acceptor functional group is required to alter the electronic structure of SWCNTs. The absorption, Raman, and STS dI/dV spectra of the surfactant peptide/SWCNT composites clearly indicate that SP-*p*NH₂F has a greater ability to interact with the SWCNT surface and to alter SWCNT electronic properties than SPF or SP-*p*CNF.

Further, the observed Raman tangential band shifts and the observed additional features near the Fermi level in the STS dI/dV spectra of the surfactant peptide/SWCNT composites were more prominent than those reported for α -helical peptide/SWCNT composites. These results verify the efficacy of the surfactant peptides to functionalize SWCNTs, presumably arising from their simple structure and the unhindered aromatic amino acid positioned at the *N*-terminus of the peptide.

Altogether, this study describes a simple peptide structure which is ideal for exploring the effect of individual functional groups on SWCNT electronic properties. A more precise knowledge of the impact of different functional groups on SWCNT properties would be useful in developing peptide/SWCNT composites with better altered electronic properties for

the design of tunable nanoscale electronic devices, such as field effect transistor-based biosensors.

Acknowledgements

The support for this project by a Young Investigator's Grant from the Human Frontier Science Program (GRD; grant RGY0070/2005-C) is greatly appreciated.

Notes and references

- 1 M. S. Dresselhaus, G. Dresselhaus, J. C. Charlier and E. Hernandez, *Philos. Trans. R. Soc. London, Ser. A*, 2004, **362**, 2065.
- 2 M. Endo, M. S. Strano and P. M. Ajayan, in *Carbon Nanotubes: Advanced Topics in the Synthesis, Structure, Properties and Applications*, ed. A. Jorio, G. Dresselhaus and M. S. Dresselhaus, Springer-Verlag, Berlin, 2008, pp. 531–566.
- 3 D. W. H. Fam, A. Palaniappan, A. I. Y. Tok, B. Liedberg and S. M. Moochhala, *Sens. Actuators, B*, 2011, **157**, 1.
- 4 P. Sharma and P. Ahuja, *Mater. Res. Bull.*, 2008, **43**, 2517.
- 5 K. Balasubramanian and M. Burghard, *J. Mater. Chem.*, 2008, **18**, 3071.
- 6 C. Gao, Z. Guo, J.-H. Liu and X.-J. Huang, *Nanoscale*, 2012, **4**, 1948.
- 7 M. Terrones, A. Filho and A. Rao, in *Carbon Nanotubes: Advanced Topics in the Synthesis, Structure, Properties and Applications*, ed. A. Jorio, G. Dresselhaus and M. S. Dresselhaus, Springer-Verlag, Berlin, 2008, pp. 531–566.
- 8 H.-J. Shin, S. M. Kim, S.-M. Yoon, A. Benayad, K. K. Kim, S. J. Kim, H. K. Park, J.-Y. Choi and Y. H. Lee, *J. Am. Chem. Soc.*, 2008, **130**, 2062.
- 9 A. K. Manna and S. K. Pati, *Nanoscale*, 2010, **2**, 1190.
- 10 C. N. R. Rao and R. Voggu, *Mater. Today*, 2010, **13**, 34.
- 11 U. Dettlaff-Weglikowska, G. Kim, L. G. Bulusheva and S. Roth, *Phys. Status Solidi B*, 2011, **248**, 2458.
- 12 A. M. Rao and P. C. Eklund, *Nature*, 1997, **388**, 257.
- 13 W. Liang, J. Yang and J. Sun, *Appl. Phys. Lett.*, 2005, **86**, 223113.
- 14 S.-S. Yu and W.-T. Zheng, *Nanoscale*, 2010, **2**, 1069.
- 15 P. Ayala, R. Arenal, M. Rummeli, A. Rubio and T. Pichler, *Carbon*, 2010, **48**, 575.
- 16 K. E. Wise, C. Park, E. J. Siochi and J. S. Harrison, *Chem. Phys. Lett.*, 2004, **391**, 207.
- 17 M. Shim, T. Ozel, A. Gaur and C. Wang, *J. Am. Chem. Soc.*, 2006, **128**, 7522.
- 18 M. Giulianini, E. R. Waclawik, J. M. Bell, M. Scarselli, P. Castrucci, M. De Crescenzi and N. Motta, *Appl. Phys. Lett.*, 2009, **95**, 143116.
- 19 V. Z. Poenitzsch, D. C. Winters, H. Xie, G. R. Dieckmann, A. B. Dalton and I. H. Musselman, *J. Am. Chem. Soc.*, 2007, **129**, 14724.
- 20 V. Zorbas, A. L. Smith, H. Xie, A. Ortiz-Acevedo, A. B. Dalton, G. R. Dieckmann, R. K. Draper, R. H. Baughman and I. H. Musselman, *J. Am. Chem. Soc.*, 2005, **127**, 12323.
- 21 D. A. Tsybouski, E. L. Bakota, L. S. Witus, J.-D. R. Rocha, J. D. Hartgerink and R. B. Weisman, *J. Am. Chem. Soc.*, 2008, **130**, 17134.
- 22 G. R. Dieckmann, A. B. Dalton, P. A. Johnson, J. Razal, J. Chen, G. M. Giordano, E. Muñoz, I. H. Musselman, R. H. Baughman and R. K. Draper, *J. Am. Chem. Soc.*, 2003, **125**, 1770.
- 23 Z. Kuang, S. N. Kim, W. J. Crookes-Goodson, B. L. Farmer and R. R. Naik, *ACS Nano*, 2009, **4**, 452.
- 24 K. A. Drouvalakis, S. Bangsaruntip, W. Hueber, L. G. Kozar, P. J. Utz and H. Dai, *Biosens. Bioelectron.*, 2008, **23**, 1413.
- 25 H. Xie, E. J. Becraft, R. H. Baughman, A. B. Dalton and G. R. Dieckmann, *J. Pept. Sci.*, 2008, **14**, 139.
- 26 C. Hansch, A. Leo and R. W. Taft, *Chem. Rev.*, 1991, **91**, 165.
- 27 D. A. Wellings and E. Atherton, in *Methods in Enzymology: Solid Phase Peptide Synthesis*, ed. G. B. Fields, Academic Press Limited, London, 1997, vol. 289, pp. 44–67.
- 28 R. W. Woody, in *The Peptides*, ed. V. J. Hruby, Academic Press Inc, Orlando, FL, 1985, vol. 7, pp. 30–42.
- 29 K. Yurekli, C. A. Mitchell and R. Krishnamoorti, *J. Am. Chem. Soc.*, 2004, **126**, 9902.
- 30 V. Z. Poenitzsch and I. H. Musselman, *Microsc. Microanal.*, 2006, **12**, 221.
- 31 V. Zorbas, A. Ortiz-Acevedo, A. B. Dalton, M. M. Yoshida, G. R. Dieckmann, R. K. Draper, R. H. Baughman, M. Jose-Yacamán and I. H. Musselman, *J. Am. Chem. Soc.*, 2004, **126**, 7222.
- 32 A. Ortiz-Acevedo, H. Xie, V. Zorbas, W. M. Sampson, A. B. Dalton, R. H. Baughman, R. K. Draper, I. H. Musselman and G. R. Dieckmann, *J. Am. Chem. Soc.*, 2005, **127**, 9512.
- 33 P. Nikolaev, M. J. Bronikowski, R. K. Bradley, F. Rohmund, D. T. Colbert, K. A. Smith and R. E. Smalley, *Chem. Phys. Lett.*, 1999, **313**, 91.
- 34 S. M. Bachilo, M. S. Strano, C. Kittrell, R. H. Hauge, R. E. Smalley and R. B. Weisman, *Science*, 2002, **298**, 2361.
- 35 M. J. O'Connell, S. M. Bachilo, C. B. Huffman, V. C. Moore, M. S. Strano, E. H. Haroz, K. L. Rialon, P. J. Boul, W. H. Noon, C. Kittrell, J. Ma, R. H. Hauge, R. B. Weisman and R. E. Smalley, *Science*, 2002, **297**, 593.
- 36 L. M. Woods, S. C. Badescu and T. L. Reinecke, *Phys. Rev. B: Condens. Matter Mater. Phys.*, 2007, **75**, 155415.
- 37 R. B. Weisman and S. M. Bachilo, *Nano Lett.*, 2003, **3**, 1235.
- 38 R. A. Sivarajan, <http://www.carbonwall.com>, accessed 05 March 2010.
- 39 H. Huang, H. Kajiura, R. Maruyama, K. Kadono and K. Noda, *J. Phys. Chem. B*, 2006, **110**, 4686.
- 40 F. Bonaccorso, *Int. J. Photoenergy*, 2010, **2010**, 727134.
- 41 N. Nair, M. L. Usrey, W.-J. Kim, R. D. Braatz and M. S. Strano, *Anal. Chem.*, 2006, **78**, 7689.
- 42 M. S. Dresselhaus, G. Dresselhaus, A. Jorio, A. G. Souza Filho and R. Saito, *Carbon*, 2002, **40**, 2043.
- 43 A. Ghosh, K. V. Rao, R. Voggu and S. J. George, *Chem. Phys. Lett.*, 2010, **488**, 198.
- 44 R. B. Koizhaiganova, D. H. Hwang, C. J. Lee, S. Roth and U. Dettlaff-Weglikowska, *Phys. Status Solidi B*, 2010, **247**, 2793.
- 45 A. Ghosh, K. V. Rao, S. J. George and C. N. R. Rao, *Chem.–Eur. J.*, 2010, **16**, 2700.
- 46 T. W. Odom, J.-L. Huang and C. M. Lieber, *J. Phys.: Condens. Matter*, 2002, **14**, R145.
- 47 L. C. Venema, *Electronic Structure of Carbon Nanotubes*, Delft University Press, Netherlands, 1999, pp. 1–63.
- 48 M. L. Terranova, S. Orlanducci, A. Serra, D. Manno, E. Filippo and M. Rossi, *Chem. Phys. Lett.*, 2011, **509**, 152.
- 49 J. W. G. Wildoer, L. C. Venema, A. G. Rinzier, R. E. Smalley and C. Dekker, *Nature*, 1998, **391**, 59.
- 50 C. Dekker, S. J. Tans, B. Oberdorff, R. Meyer and L. C. Venema, *Synth. Met.*, 1997, **84**, 853.
- 51 P. G. Collins, K. Bradley, M. Ishigami and A. Zettl, *Science*, 2000, **287**, 1801.
- 52 <http://www.phy.ohiou.edu/~asmith/NewATOMS/HOPG.pdf>, accessed 20 May 2010.
- 53 A. V. Naumov, O. A. Kuznetsov, A. R. Harutyunyan, A. A. Green, M. C. Hersam, D. E. Resasco, P. N. Nikolaev and R. B. Weisman, *Nano Lett.*, 2009, **9**, 3203.
- 54 R. Czerw, M. Terrones, J. C. Charlier, X. Blase, B. Foley, R. Kamalakaran, N. Grobert, H. Terrones, D. Tekleab, P. M. Ajayan, W. Blau, M. Ruhle and D. L. Carroll, *Nano Lett.*, 2001, **1**, 457.
- 55 M. Terrones, A. Jorio, M. Endo, A. M. Rao, Y. A. Kim, T. Hayashi, H. Terrones, J. C. Charlier, G. Dresselhaus and M. S. Dresselhaus, *Mater. Today*, 2004, **7**, 30.
- 56 T. W. Odom, J.-L. Huang, P. Kim and C. M. Lieber, *J. Phys. Chem. B*, 2000, **104**, 2794.
- 57 L. Yang and J. Han, *Phys. Rev. Lett.*, 2000, **85**, 154.